

Prompt fission neutron spectra in fast-neutron-induced fission of ^{238}U V. V. Desai,^{1,*} B. K. Nayak,^{1,†} A. Saxena,¹ S. V. Suryanarayana,¹ and R. Capote²¹*Nuclear Physics Division, Bhabha Atomic Research Centre, 400 085 Mumbai, India*²*NAPC—Nuclear Data Section, International Atomic Energy Agency, A-1400 Vienna, Austria*

(Received 7 April 2015; revised manuscript received 9 June 2015; published 8 July 2015)

Prompt fission neutron spectrum (PFNS) measurements for the neutron-induced fission of ^{238}U are carried out at incident neutron energies of 2.0, 2.5, and 3.0 MeV, respectively. The time-of-flight technique is employed to determine the energy of fission neutrons. The prompt fission neutron energy spectra so obtained are analyzed using Watt parametrization to derive the neutron multiplicity and average prompt fission neutron energy. The present experimental PFNS data are compared with the evaluated spectra taken from the ENDF/B-VII.1 library and the predictive calculations carried out using the EMPIRE-3.2 (Malta) code with built-in Los Alamos (LA) and Kornilov PFNS models. The sensitivity of the EMPIRE-3.2 LA model—calculated PFNS to the nuclear level density parameter of the average fission fragment and to the total kinetic energy is investigated. EMPIRE-3.2 LA model PFNS calculations that use Madland 2006—recommended values [D. G. Madland, *Nucl. Phys. A* **772**, 113 (2006)] of the total kinetic energy and the level density parameter $a = A/(10 \pm 0.5)$ compare very well to measured data at all incident neutron energies.

DOI: 10.1103/PhysRevC.92.014609

PACS number(s): 25.85.Ec, 24.75.+i

I. INTRODUCTION

Studies on prompt fission neutron spectra properties in neutron-induced fission reactions, taking place at from low to intermediate energies, have grown increasingly popular in recent years due to the worldwide interest in the design of fast breeder reactors and development of accelerator-driven systems for the transmutation of nuclear wastes and also for the evaluation of nuclear data for actinide nuclei. Moreover, these data provide valuable information on the fundamental understanding of the neutron-induced fission process. In particular, it is interesting to investigate in what proportions the heated system releases its excess energy as a function of the incident neutron energy. There are limited experimental studies on prompt fission neutron spectra for fast-neutron-induced fission [1]. This situation is mainly due to the following difficulties: (a) small fission cross sections for fast neutrons; (b) the large background produced in the same energy region as that of fission neutrons due to scattering of incident neutrons; and (c) the fact that a monoenergetic neutron source of the required energy with the appropriate intensity is often not easily accessible.

Prompt fission neutrons are characterized by two basic quantities: the average number of prompt neutrons emitted per fission, which is known up to 30 MeV with an accuracy of better than 1%, and the shape of the neutron energy spectrum, which is not nearly as well known [1]. The need for better knowledge of prompt fission neutron spectra for actinide nuclei is also reflected in the International Atomic Energy Agency (IAEA) request list [2]. In connection with the coordinated research program [3] launched by the IAEA, we have initiated a program to measure the prompt fission neutron spectrum (PFNS) in fast-neutron-induced fission of major actinides such

as ^{238}U and ^{232}Th . In this work, we report on some of the results of our research program, which focuses on measuring the PFNS emitted in the fast-neutron-induced fission of ^{238}U at incident neutron energies of 2.0, 2.5, and 3.0 MeV.

II. THEORETICAL MODELING OF PROMPT FISSION NEUTRON SPECTRA**A. Maxwellian and Watt formalism**

A commonly used approximation for fission neutron spectra in the laboratory system is the Maxwellian distribution as presented by Terrell [4,5].

$$N_M(E) = \frac{2 \cdot E^{1/2}}{\pi^{1/2} \cdot T_M^{3/2}} \times \exp\left(-\frac{E}{T_M}\right), \quad (1)$$

where T_M is the only parameter characterizing the distribution. The average neutron energy is given by

$$\bar{E} = \frac{3}{2} \cdot T_M. \quad (2)$$

If a Maxwellian distribution is assumed for the shape of the neutron evaporation spectrum, $N(E) \sim \sqrt{E} \times \exp(-E/T_e)$, where T_e is the temperature of the nucleus after the evaporation of one neutron; and furthermore, if it is assumed that all fragments have the same kinetic energy per nucleon E_f , then the laboratory neutron spectrum shape is a Watt spectrum [6,7],

$$N_w(E) = \frac{2 \cdot A^{3/2}}{(\pi \cdot B)^{1/2}} \times \exp\left(-\frac{B}{4A}\right) \times \exp(-A \cdot E) \times \sinh(B \cdot E)^{1/2}. \quad (3)$$

The Watt parameters A and B are related to the physical quantities by the relations $A = 1/T_e$ and $B = 4E_f/T_e^2$. The average neutron energy of the Watt distribution is simply given by

$$\bar{E} = \frac{1}{A} \cdot \left(\frac{3}{2} + \frac{B}{4 \cdot A}\right). \quad (4)$$

*vvdesai@barc.gov.in

†bknayak@barc.gov.in

The above Watt parametrization has a limited accuracy, but it is a useful approximation to describe a PFNS with low statistics. Also, the average neutron energy is derived analytically using Eq. (4), therefore, is not sensitive to details of the spectral shape near the chosen upper and lower thresholds.

B. Los Alamos model

The Los Alamos (LA) model is the basis for evaluation of prompt fission neutron spectra in most currently evaluated nuclear data libraries. This relatively simple and compact formalism has been very successful in predicting the prompt fission neutron spectra for neutron-induced as well as spontaneous fission reactions for a wide range of actinides and incident neutron energies. In the present work, we have used the EMPIRE-3.2 (Malta) code implementation of the LA model for PFNS calculations with the EMPIRE selection of model input parameters [8–10]. More detailed discussion of the LA model can be found in Refs. [10–14]. Here we only summarize its main features. In this model, the PFNS $N(E)$ is calculated as a function of the fissioning nucleus and its excitation energy. The Weisskopf statistical evaporation theory [15] is used to predict the emission of neutrons from an excited compound nucleus (CN) at a given temperature, and a triangular distribution of initial fission fragment residual temperatures is assumed. The equation for the center-of-mass fission neutron energy spectrum, for an energy-dependent compound-nucleus cross section and constant residual nuclear temperature, is

$$\phi(E) = \frac{2\sigma_c(\epsilon)\epsilon}{T_c^2} \int_0^{T_m} k(T)T \exp\left(-\frac{\epsilon}{T}\right) dT, \quad (5)$$

with the temperature-dependent normalization constant $k(T)$

$$k(T) = \left(\int_0^\infty \sigma_c(\epsilon)\epsilon \exp\left(-\frac{\epsilon}{T}\right) d\epsilon \right)^{-1}. \quad (6)$$

$\sigma_c(\epsilon)$ is the energy-dependent cross section for the inverse process of compound nucleus (CN) formation. Equation (7) was obtained by integrating over a triangular distribution of temperatures with a maximum temperature T_m .

In the laboratory system, the neutron energy spectrum $N(E)$ for a fission fragment moving with a kinetic energy per nucleon E_f is

$$N(E) = \frac{1}{2\sqrt{E_f T_m^2}} \int_{(\sqrt{E}-\sqrt{E_f})^2}^{(\sqrt{E}+\sqrt{E_f})^2} \sigma_c(\epsilon)\sqrt{\epsilon} d\epsilon \times \int_0^{T_m} k(T)T \exp\left(-\frac{\epsilon}{T}\right) dT. \quad (7)$$

Considering the most probable fragmentation only, the average laboratory neutron energy spectrum $N(E)$ is therefore given by an average over the spectra for the light $N_l(E)$ and heavy $N_h(E)$ fragments as

$$N(E) = \frac{1}{2}(N_l(E) + N_h(E)). \quad (8)$$

The LA model takes into account several important physical effects that the Watt or Maxwellian representation ignores, such as (i) the distribution of the fission-fragment residual nuclear temperature that results from the initial distribution

of the fission-fragment excitation energy and the subsequent cooling of the fragments as neutrons are emitted and (ii) the energy dependence of the cross section for the inverse process of compound nucleus formation. Furthermore, the Maxwellian spectrum also neglects the center-of-mass motion of the fission fragments from which the neutrons are emitted; therefore, the agreement between spectra and data is achieved by adjusting parameters to values that are somewhat unphysical. The LA model addresses these inconsistencies by taking the distribution of the fission-fragment residual nuclear temperature to be triangular in shape, extending linearly from 0 to a maximum value T_m , and calculating the energy-dependent compound nucleus cross section for representative average fission fragments by the use of an optical model. This permits $N(E)$ to be calculated easily for any fissioning nucleus at any excitation energy.

III. EXPERIMENTAL DETAILS AND DATA ANALYSIS

The experiment was performed at the 6-MV Folded Tandem Ion Accelerator facility [16], Bhabha Atomic Research Centre, Mumbai, India. The primary monoenergetic neutrons were obtained via ${}^7\text{Li}(p,n){}^7\text{Be}$ reaction by bombarding the proton beam on a natural ${}^7\text{Li}$ metallic target of thickness 4.0 mg/cm^2 ($1.0 \times 1.0\text{-cm}$ area). The absolute differential cross sections of the ${}^7\text{Li}(p,n){}^7\text{Be}$ and ${}^7\text{Li}(p,n_1){}^7\text{Be}^*$ reactions were measured earlier for proton energies from 2.20 to 5.50 MeV [17]. The contribution of this second group of neutrons from the ${}^7\text{Li}(p,n_1){}^7\text{Be}^*$ reaction is less than 10% at all incident neutron energies reported in this work. A schematic of the experimental arrangement is shown in Fig. 1. A fission chamber used for fission-fragment detection was placed downstream at a distance of 2.0 cm from the neutron production target ${}^7\text{Li}$ as shown in Fig. 1. The fission chamber is made up of two circular pcb plates (7 cm in diameter and 2 mm thick) arranged in parallel with a 3.0-mm spacer of Teflon ring between them. The natural ${}^{238}\text{U}$ (99.30%) target of thickness

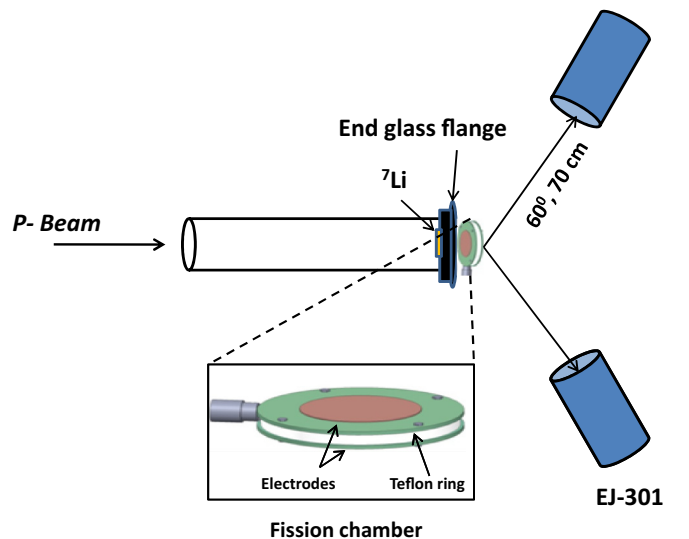


FIG. 1. (Color online) Schematic of the experimental setup.

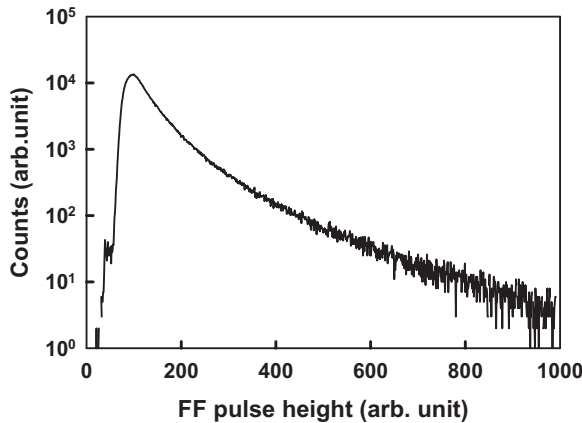


FIG. 2. Fission fragment (FF) pulse height spectrum.

2.1 mg/cm² (1.0 × 1.0-cm area) was mounted on the cathode plate of a fission chamber with an electrical contact made using a conducting glue. The ²³⁸U target mounted in the fission chamber subtended an angular opening of ±14° at the center of the neutron production target. Thus incident neutrons falling on the ²³⁸U target will have some energy spread. The spread in the incident neutron energy is determined from the angular opening presented by the ²³⁸U target at the center of the neutron production target and it is found to be ~100 keV at all incident neutron energies. The produced neutrons are allowed to fall on a ²³⁸U target mounted on the cathode plate of a fission chamber. The fission fragments produced in the ²³⁸U(*n, f*) reaction are detected in 2π geometry in the fission chamber. The cathode plate was kept at ground potential, while the anode was biased to 600 V through a preamplifier. The fission fragments ionize the air between the two plates, generating electron-ion pairs. The generated electron-ion pairs are then collected at their respective electrodes, leading to an electrical pulse, signing a fission event which is then used as a start pulse for the time-of-flight (TOF) measurement. The discrimination among fission-fragment pulse height, α-particle energy loss (²³⁸U is an α emitter), and electronic noise was excellent. The typical fission-fragment pulse height spectrum is shown in Fig. 2. The threshold is applied during the off-line analysis so as to discard any random coincidences caused by the trigger's arising from α and the electronic noise in the fission chamber.

Two EJ301 liquid organic scintillator detectors (12.7 cm in diameter and 5.0 cm thick), sensitive to neutrons and γ rays, were placed at a distance of 70.0 cm from the center of the fission chamber, making an angle of 60° with respect to the incident neutron beam direction on either side of the beam to detect fission neutrons. The neutron detectors were mounted on the flat aluminum platform coupled with a tripod stand. The distance of the walls of the experimental room from the neutron detectors is about 10 m. Both neutron detectors were set up with the ¹³⁷Cs, ⁶⁰Co, and ²²Na calibration sources to set the electronic thresholds at a 30-keV electron equivalent energy. The signal of the neutron (or γ ray) hitting the EJ301 detector is used as a stop signal for TOF measurement. The EJ301 exhibits good pulse shape discrimination (PSD) properties, therefore, neutrons and γ rays can be discriminated via a pulse

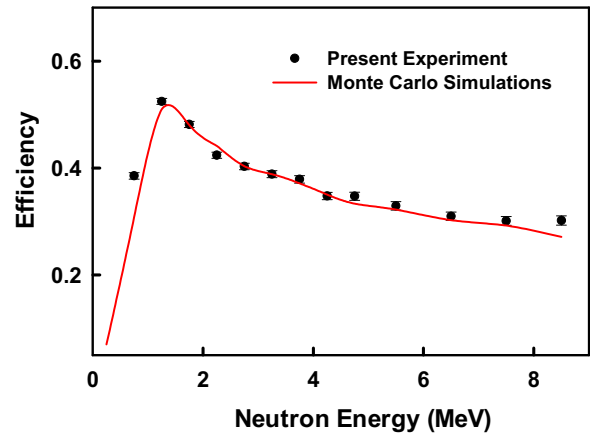


FIG. 3. (Color online) Measured efficiency for the EJ301 neutron detectors.

shape analysis using a Mesytec MPD-4 module [18] based on the charge integration of the short- and long-decay-time components of the scintillation detector pulses.

The detection efficiency of each of the neutron detectors was experimentally determined in a separate experiment by measuring the neutron TOF spectrum in coincidence with fission fragments from a ²⁵²Cf source. The ²⁵²Cf source was mounted on the cathode electrode of the fission chamber, hence the fission fragments were detected in 2π geometry (identical to the above in-beam experiment with the ²³⁸U target). The neutron energy spectrum measured per fission is then compared with the empirical form provided by Mannhart evaluation [19,20], which is considered the standard for ²⁵²Cf(SF). Figure 3 and Table I present the measured efficiency of the detectors. The calculated efficiency using the NEFF code is also shown in Fig. 3, for comparison. However, the measured efficiency has been used in analysis of the present data.

A two-dimensional PSD-versus-TOF plot and the resulting neutron TOF distribution are shown in Figs. 4(a) and 4(b), respectively. Other than the prompt neutron peak, a constant background is observed in the TOF spectrum. The prompt peak is due to the neutrons emitted in the ²³⁸U(*n, f*) reaction and the non-negligible background component arising mainly from scattered incident neutrons. These neutrons are not correlated with fission and create the constant background in the neutron

TABLE I. Efficiency correction parameters for prompt energy bins used in the present data.

Neutron energy (MeV)	Efficiency	Neutron energy (MeV)	Efficiency
0.5–1.0	0.3853 ± 0.00311	4.0–4.5	0.3477 ± 0.00340
1.0–1.5	0.5362 ± 0.00283	4.5–5.0	0.3472 ± 0.00376
1.5–2.0	0.4815 ± 0.00290	5.0–6.0	0.3292 ± 0.00391
2.0–2.5	0.4239 ± 0.00289	6.0–7.0	0.3098 ± 0.00387
2.5–3.0	0.4030 ± 0.00301	7.0–8.0	0.3010 ± 0.00410
3.0–3.5	0.3885 ± 0.00323	8.0–9.0	0.3019 ± 0.00435
3.5–4.0	0.3788 ± 0.00346		

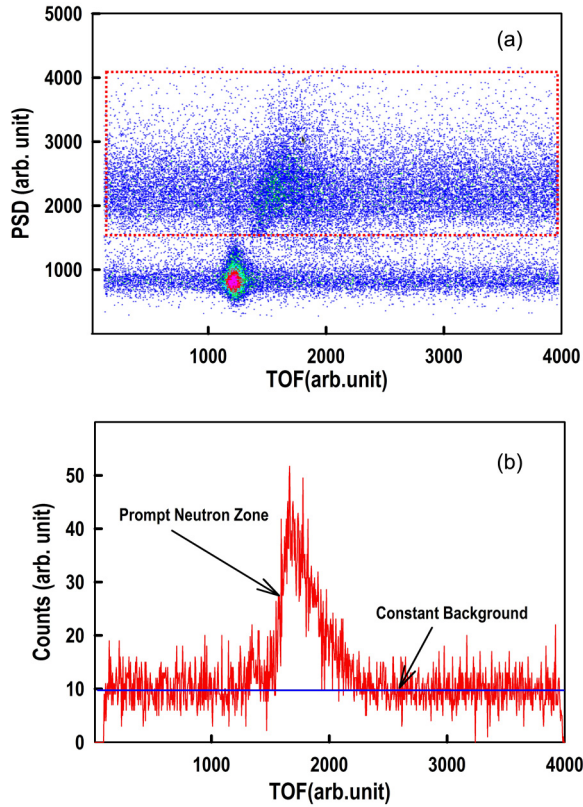


FIG. 4. (Color online) (a) Typical two-dimensional pulse shape discrimination (PSD) vs time-of-flight (TOF) plot; (b) neutron TOF spectrum.

TOF spectra through random coincidences. The TOF spectra are then converted into energies using the relativistic equation

$$E_n = m_n c^2 \left[\frac{1}{\sqrt{1 - \frac{v_n^2}{c^2}}} - 1 \right], \quad (9)$$

where E_n , v_n , and m_n are the energy, velocity, and mass of the neutron and c is the speed of the light. First, the neutron energy spectrum is generated for the coincidence region (prompt neutron zone in Fig. 4(b)) of TOF spectra. An energy spectrum corresponding to a constant background of a width similar to the coincidence region of the TOF is also generated by appropriately shifting the time scale. In order to obtain the true coincident neutron spectrum, the neutron energy spectra corresponding background region is subtracted from the coincidence region. The spectrum is then normalized to the number of fission events and the solid angle of the neutron detector and corrected with the measured neutron detection efficiency shown in Fig. 3. The resulting PFNS energy distributions so obtained at $E_n = 2.0, 2.5,$ and 3.0 MeV are shown in Figs. 5(a), 5(b), and 5(c), respectively. The data show both detectors added together for better statistics. The error bars on the y axis contain statistical uncertainties in the neutron yield measurement itself.

The systematic uncertainties associated with PFNS data measurements using the modern approach have been presented and discussed briefly in the work of Rising *et al.* [21] and

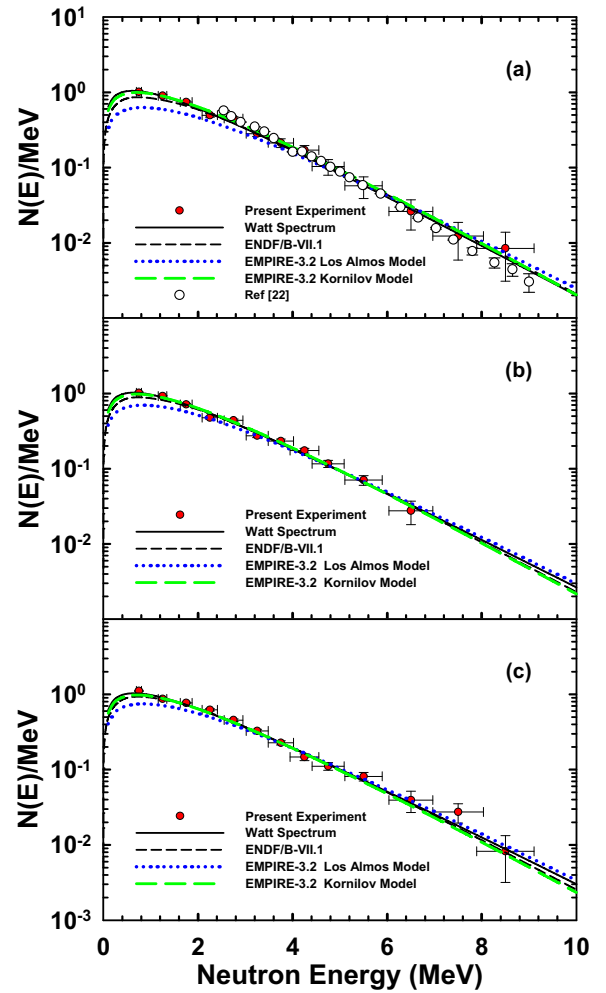


FIG. 5. (Color online) Comparison of prompt fission neutron spectra among the present experimental data, Watt spectrum (solid line), ENDF/B-VII.1 evaluation (short-dashed line), EMPIRE-3.2 Los Alamos model (dotted line), and Kornilov model (long-dashed line) at incident neutron energies of (a) 2.0 MeV, (b) 2.5 MeV, and (c) 3.0 MeV.

Neudecker *et al.* [22]. The systematic uncertainties in the present data include uncertainties in the detector efficiency measurements and uncertainty in the separation of neutron and γ events by PSD and in the background subtraction. The neutron detection efficiencies for the neutron detectors have been determined using the ^{252}Cf source as described above. Figure 3 shows a comparison between the measured efficiency and the calculated efficiency using the NEFF Monte Carlo simulation code. Near the threshold for neutron detection, the uncertainty in the detector efficiency measurements is somewhat greater. However, for the data reported in the present work for emitted neutron energies above 1 MeV, the 5% uncertainty is appropriate. The neutron- γ discrimination is quite clean; therefore the uncertainty in identifying neutron and γ events by PSD is negligible. The constant background shown in the TOF spectra in Fig. 4(b) due to the random coincidences formed by scattered incident neutrons was subtracted carefully as described earlier. The uncertainty in the neutron spectra due

TABLE II. Best-fit values of fitting parameters in Maxwellian and Watt parametrization. Extracted values of the neutron multiplicity and average neutron energy are also listed.

E_n (MeV)	Watt fit				Maxwellian fit			\bar{E} ($0.75 \leq E \leq 7.5$)
	A (MeV^{-1})	B (MeV^{-1})	M_n	\bar{E}	T (MeV)	M_n	\bar{E}	
2.0	0.819 ± 0.005	1.20 ± 0.002	2.59 ± 0.020	2.28 ± 0.017	1.24 ± 0.01	2.59 ± 0.025	1.86 ± 0.015	2.24 ± 0.034
2.5	0.784 ± 0.003	0.994 ± 0.002	2.62 ± 0.020	2.30 ± 0.018	1.27 ± 0.01	2.62 ± 0.025	1.90 ± 0.015	2.26 ± 0.028
3.0	0.751 ± 0.005	0.892 ± 0.002	2.72 ± 0.025	2.31 ± 0.020	1.29 ± 0.01	2.62 ± 0.025	1.92 ± 0.015	2.27 ± 0.041

to background subtraction is less than 12%. The scattering of fission neutrons from the components of the fission chamber, the detector mounts, and the wall of the experimental room can contribute to lower emission energies of the neutron spectrum. This requires more detailed study through simulations to understand the contribution to the neutron emission spectrum due to scattering from the structural material of the fission chamber, detector mounts, and walls of the experimental room, as the information given above.

IV. RESULTS AND DISCUSSION

The Watt parametrization given by Eq. (3) and the EMPIRE-3.2 (Malta) code implementation of the LA model [8–10] and Kornilov model [23] calculations have been performed to quantitatively understand the present experimental PFNS data. Figures 5(a)–5(c) show the present prompt fission neutron spectra along with the best-fit line of the Watt spectrum, EMPIRE-3.2 LA model, Kornilov model calculations, and evaluated PFNS taken from the ENDF/B-VII.1 library [24]. The best-fit values of the Watt parameters A and B and prompt fission neutron multiplicity (M_n), obtained by fitting the observed spectra by the χ^2 minimization procedure, are listed in Table II. The two calculations (Watt spectrum and Kornilov model) and the evaluated spectra model, and the evaluated PFNS taken from the ENDF/B-VII.1 library show the same trend as the experimental data. However, the PFNS calculated using the EMPIRE-3.2 LA model gives lower values at low emission energies than the other data plotted in Fig. 5 at all incident neutron energies. In Fig. 5(a), the data reported by Baba *et al.* [25] at 2.0 MeV are shown for comparison. The data reported by Baba *et al.* at 2.0 MeV are found to be consistent with the present data in the emission neutron energy range of 2.5 to 7.0 MeV. However, above 7.0 MeV, the Baba *et al.* data deviate slightly from the present data. In Fig. 6(a), the values of the multiplicities (M_n) deduced in the present experiment are compared with other experimental data taken from the EXFOR [26] library and evaluations taken from the ENDF/B-VII.1 library [24]. The multiplicity values obtained in the present work at all incident neutron energies are found to be consistent with the earlier experimental data as well as the ENDF/B-VII.1 evaluation. The average prompt fission neutron energy (\bar{E}) values calculated from the fitted parameters using Eq. (4) are also listed in Table II. Figure 6(b) shows a comparison of the average prompt fission neutron energy \bar{E} values obtained in the present work with the previously reported data taken from Ref. [27] and the LA model calculations. In general, the average PFNS energy

data along with the present measurement plotted in Fig. 6(b) show a slightly increasing behavior with the incident beam neutron energy. The present experimental \bar{E} data at all incident neutron energies are consistent with the earlier experimental data and the LA model calculations. The spectrum average neutron energy in the energy range $0.75 \leq E_n \leq 7.5$ is also shown in Fig. 6(b). The prompt fission neutron energy spectra obtained in the present experiment also have been fitted by the Maxwellian distribution given by Eq. (1). The Maxwellian temperature (T_M) and multiplicity (M_n) have been deduced by least-squares fit. The best-fit values of the Maxwellian parameters (T_M) and (M_n) and hence the average energy (\bar{E}) obtained in the present work for incident energies of 2.0, 2.5,

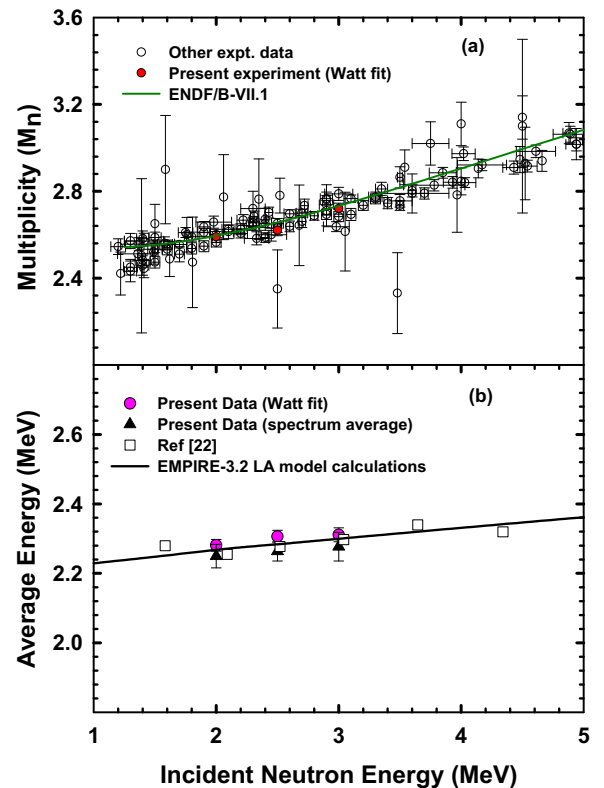


FIG. 6. (Color online) (a) Average neutron multiplicity: present data (filled circles) and other experimental data (open circles) taken from EXFOR and ENDF/B-VII.1 evaluation (solid line). (b) Prompt fission neutron spectrum average energy (\bar{E}) for neutrons emitted from neutron-induced fission of ^{238}U . Data are compared with previously reported experimental data and also with predictions of EMPIRE-3.2 Los Alamos model calculations.

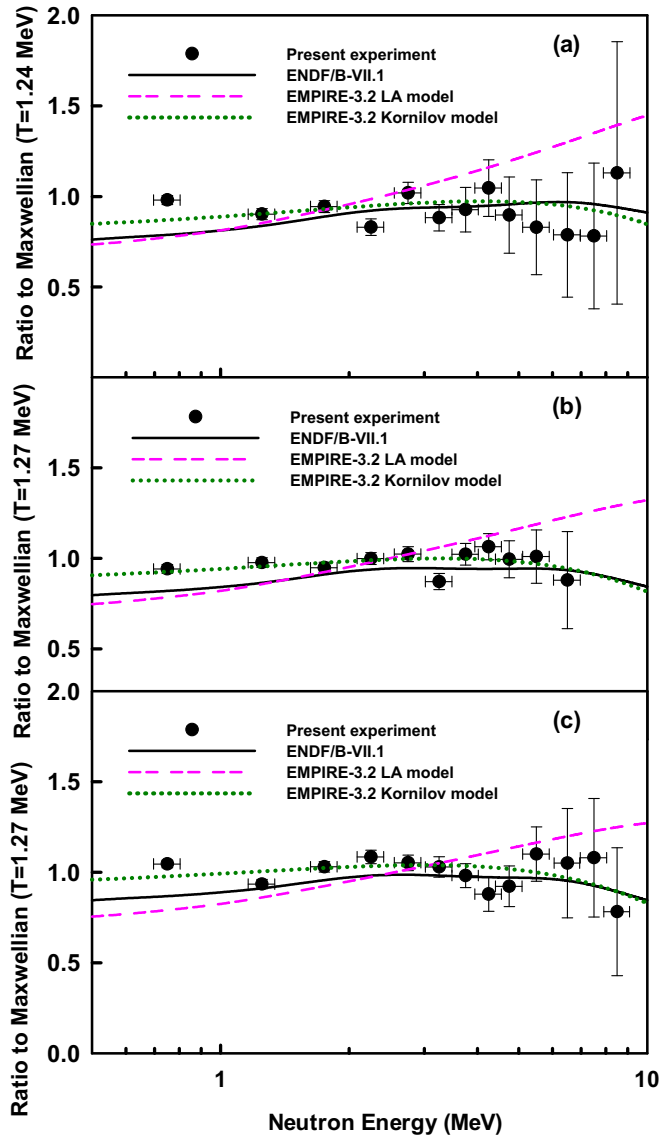


FIG. 7. (Color online) Experimental (open circles) and calculated [ENDF/B-VII.1 evaluation (solid line), EMPIRE-3.2 Los Alamos model (short-dashed line), and Kornilov model (dotted line)] prompt fission neutron energy spectra, normalized to the Maxwellian distribution at an incident neutron energy of (a) 2.0 MeV, (b) 2.5 MeV, and (c) 3.0 MeV.

and 3.0 MeV are listed in Table II. The ratio of the experimental and calculated PFNS normalized to the respective Maxwellian distribution is shown in the Fig. 7. In this way the shapes of the prompt fission neutron spectra are compared. It can be seen in Fig. 7 that the shapes of the evaluated spectra taken from the ENDF/B-VII.1 library and the calculated PFNS using the Kornilov model are consistent with the present experimental data at all incident neutron energies. However, the shape of the PFNS predicted by the EMPIRE-3.2 LA model implementation is considerably different from the present experimental data.

The sensitivity of the PFNS calculations to the perturbation of model input parameters for the EMPIRE-3.2 LA model has been carried out to understand the observed difference between

TABLE III. Comparison of average total kinetic energies of fission fragment values used in the default EMPIRE-3.2 parametrization and values obtained from the Madland systematics.

Incident neutron energy (MeV)	$\langle T_f^{\text{tot}} \rangle$ (MeV)	
	EMPIRE-3.2	Madland systematic
2.0	168.68	171.24
2.5	168.29	171.12
3.0	168.10	171.02

the present experimental and the LA-calculated spectral shape. The relevant input parameters for the LA model are (i) $\langle E_r \rangle$, the average fission energy release; (ii) $\langle S_n \rangle$, the average neutron separation energy of the fission fragments; (iii) $\langle T_f^{\text{tot}} \rangle$, the total kinetic energy of the fission fragments; and (iv) $\langle E_\gamma^{\text{tot}} \rangle$, the average total energy carried away through γ -ray emission. The EMPIRE-3.2 implementation of the LA model calculations in the present work have been carried out with the EMPIRE selection of model input parameters. The default parameters used in EMPIRE for the LA model of prompt fission neutron emission in $^{238}\text{U}(n_{\text{th}}, f)$ reactions have been taken from the work of Malinovskii *et al.* [28] and Itkis *et al.* [29]. Also, for the level density parameter a , the EMPIRE-3.2 implementation of the PFNS calculation uses the relationship

$$a = A/11 \text{ (MeV)}, \quad (10)$$

where A is the mass number of the most probable heavy and light fission fragments for the $n + ^{238}\text{U}$ reaction. The sensitivity of the EMPIRE-3.2 LA model-predicted PFNS to the perturbation of the total kinetic energy $\langle T_f^{\text{tot}} \rangle$ of fission fragments has been studied by taking the $\langle T_f^{\text{tot}} \rangle$ values from the systematics suggested by Madland [30] over the incident neutron energy (E_n) range of $0 \leq E_n \leq 30$ as given below:

$$\langle T_f^{\text{tot}} \rangle = 171.7 - 0.2396E_n + 0.003434E_n^2. \quad (11)$$

The above systematic was obtained by a fit to the published experimental average total fission fragment kinetic energy data for the $n + ^{238}\text{U}$ system by Zoller *et al.* [31]. The EMPIRE-3.2 parametrization of the LA model uses the $\langle T_f^{\text{tot}} \rangle$ parametrization proposed by Malinovskii *et al.* [28]. A comparison of the average total fission fragment kinetic energy $\langle T_f^{\text{tot}} \rangle$ values used in the default EMPIRE-3.2 parametrization and the values obtained from the systematic given by Eq. (17) are listed in Table III. Figure 8 shows the EMPIRE-3.2 LA model-calculated prompt fission neutron spectra obtained using the $\langle T_f^{\text{tot}} \rangle$ values from the above systematic and the EMPIRE-3.2 selected level density parameter $a = A/11$ (MeV). To further investigate the sensitivity to the level density parameter, the ratio of the EMPIRE-3.2 LA model-predicted PFNS to the Maxwellian distribution was carried out for various values of the level density parameter a , such as $\frac{A}{9}$, $\frac{A}{9.5}$, and $\frac{A}{10}$, respectively, and the corresponding results are shown in Fig. 8. The least χ^2 method was used to extract the most probable value of the level density parameter. From Fig. 8 it appears that the present experimental data could be explained well using the EMPIRE-3.2 LA model calculations when the values of $\langle T_f^{\text{tot}} \rangle$ are

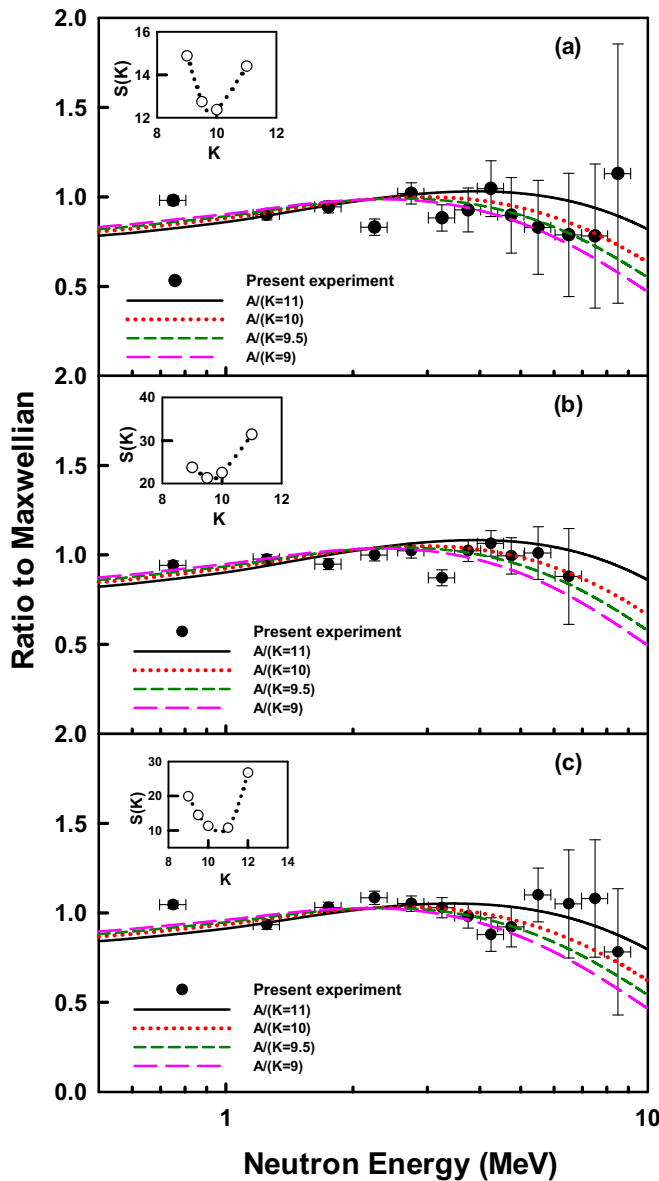


FIG. 8. (Color online) Experimental (open circles) and EMPIRE-3.2 LA model-calculated PFNS spectra obtained using the $\langle T_f^{\text{tot}} \rangle$ values taken from the Madland systematic (solid line), normalized to the Maxwellian distribution at an incident neutron energy of 2.0, 2.5, and 3.0 MeV. The effect of changing the level density parameter value is also shown.

taken from the Madland systematic given by Eq. (17) and the level density parameter $a = A/K$, where $K = 10. \pm 0.5$ MeV is used, at all incident neutron energies. Indeed the prompt fission spectrum in ENDF/B-VII.1 [24] for ^{238}U also came from a new analysis by Madland [30] using the LA model.

V. SUMMARY

The prompt fission neutron spectra from neutron-induced fission of ^{238}U have been measured using the TOF technique for incident neutron energies of 2.0, 2.5, and 3.0 MeV. A beam of primary quasimonoenergetic neutrons was obtained using the $^7\text{Li}(p,n)^7\text{Be}$ reaction. Neutrons emitted in the $^{238}\text{U}(n,f)$ reactions were detected using an EJ-301 liquid scintillator detector in coincidence with the fission fragments. The present experimental PFNS data were then compared with the Watt parametrization, ENDF/B-VII.1 evaluations, and theoretical predictions using the EMPIRE-3.2 (Malta) code with its built-in LA model and Kornilov model for PFNS calculations. The present experimental PFNS data agree very well with the Watt parametrization, ENDF/B-VII.1 evaluations, and Kornilov model for incident neutron energies of 2.0, 2.5, and 3.0 MeV. However, a significant difference between the present PFNS data and the calculated spectra using the EMPIRE-3.2 LA model is observed at all incident neutron energies. In order to understand the observed difference between the present experimental and the EMPIRE-3.2 LA-calculated spectra, a sensitivity study of PFNS calculations to perturbation of the total kinetic energy $\langle T_f^{\text{tot}} \rangle$ of fission fragments and the value of the level density parameter a used in the EMPIRE-3.2-implemented LA model calculations has been carried out. It was found that the EMPIRE-3.2 LA model-calculated prompt fission neutron spectra compare very well with the present experimental data, when $\langle T_f^{\text{tot}} \rangle$ are taken from the Madland systematic and the level density parameter $a = A/K$, where $K = 10. \pm 0.5$ MeV is used, at all incident neutron energies.

ACKNOWLEDGMENTS

The authors thank the operating staff of the Folded Tandem Ion Accelerator facility, Bhabha Atomic Research Centre, Mumbai, for smooth operation of the accelerator during the experiment. We are also thankful to Drs. R. K. Choudhury and S. Ganesan for the discussion of various aspects of this work and the constant encouragement.

[1] J. Frehaut, *Proceedings, Transactinium Isotope Neutron Data Measurements, IAEA-TECDOC-336, Uppsala 1984* (International Atomic Energy Agency, Vienna, 1985), pp. 105–131.
 [2] N. Kocherov and P. K. McLaughlin, World REQUESTequest List for Nuclear Data, Rep. INDC(SEC)-104 (International Atomic Energy Agency, Vienna, 1993); <http://www.nds.iaea.org/publications/indc/indc-sec-0104.pdf>.
 [3] R. Capote Noy, V. Maslov, E. Bauge, T. Ohsawa, A. Vorobyev, M. B. Chadwick, and S. Oberstedt, Summary Report, Consultant's Meeting on Prompt Fission Neutron Spectra of Major Actinides, INDC(NDS)-0541, January (2009).

[4] J. Terrell, *Phys. Rev.* **113**, 527 (1959).
 [5] J. Terrell, *Phys. Rev.* **127**, 880 (1962).
 [6] B. E. Watt, *Phys. Rev.* **87**, 1037 (1952).
 [7] C. Wagemans, in *The Nuclear Fission Process* (CRC Press, London, 1991), pp. 497–544.
 [8] M. Herman *et al.*, *Nucl. Data Sheets* **108**, 2655 (2007).
 [9] M. Herman *et al.*, *EMPIRE-3.2 (Malta) User's Manual, INDC(NDS)-0603* (2013); <http://www.nds.iaea.org/publications/indc/indc-nds-0603.pdf>.
 [10] R. Capote *et al.*, *Nucl. Data Sheets* **110**, 3107 (2009).
 [11] D. G. Madland and J. R. Nix, *Nucl. Sci. Eng.* **81**, 213 (1982).

- [12] G. Vladuca and A. Tudora, *Ann. Nucl. Energy* **28**, 689 (2001).
- [13] S. Noda *et al.*, *Phys. Rev. C* **83**, 034604 (2011).
- [14] P. Staples, J. Egan, G. H. R. Kegel, A. Mittler, and M. L. Woodring, *Nucl. Phys. A* **591**, 41 (1995).
- [15] V. Weisskopf, *Phys. Rev.* **52**, 295 (1937).
- [16] P. Singh *et al.*, *Pramana* **59**, 739 (2002).
- [17] S. A. Elbaker, I. J. van Heerden, W. J. McDonald, and G. C. Neilson, *Nucl. Instr. Methods* **105**, 519 (1972).
- [18] Four-channel particle discriminator module for liquid scintillators, MPD-4 data sheet; www.mesytec.com/datasheets/MPD-4.pdf.
- [19] W. Mannhart, in *Proceedings of IAEA Advisory Group Meeting, Properties of Neutron Sources, TECDOC-410* (International Atomic Energy Agency, Vienna, 1987), p. 158.
- [20] W. Mannhart, INDC(NDS)-220, 305 (International Atomic Energy Agency, Vienna, 1989), pp. 305–336.
- [21] M. E. Rising, P. Talou, T. Kawano, and A. K. Prinja, *Nucl. Sci. Eng.* **175**, 81 (2013).
- [22] D. Neudecker *et al.*, *Nucl. Data Sheets* **123**, 146 (2015).
- [23] N. V. Kornilov, A. B. Kagalenko, and F.-J. Hamsch, *Phys. At. Nucl.* **62**, 173 (1999).
- [24] M. B. Chadwick *et al.*, *Nucl. Data Sheets* **107**, 2931 (2006).
- [25] M. Baba, H. Wakabayashi, N. Ito, K. Maeda, and N. Hirakawa, *J. Nucl. Sci. Technol.* **27**, 601 (1990).
- [26] EXFOR, Experimental Nuclear Reaction Data 2015; <http://www-nds.iaea.org/exfor>.
- [27] T. Ethvignot, M. Devlin, R. Drosig, T. Granier, R. C. Haight, B. Morillon, R. O. Nelson, J. M. O'Donnell, and D. Rochman, *Phys. Lett. B* **575**, 221 (2003).
- [28] V. V. Malinovskii *et al.*, INDC(CCP)-277 (International Atomic Energy Agency, Vienna, 1987).
- [29] M. G. Itkis *et al.*, *Yad. Fiz.* **52**, 23 (1990).
- [30] D. G. Madland, *Nucl. Phys. A* **772**, 113 (2006).
- [31] EXFOR, Experimental Nuclear Reaction Data 2015; <http://www-nds.indcentre.org.in/exfor/servlet/X4sGetSubent?reqx=89303&subID=22799002>.